Available online at www.sciencedirect.com

ScienceDirect

Solar Energy 116 (2015) 83–99

SOLAR ENERGY

www.elsevier.com/locate/solener

Regional and seasonal characteristics of global horizontal irradiance forecasts obtained from the Japan Meteorological Agency mesoscale model

Hideaki Ohtake [a,*], Joao Gari da Silva Fonseca Jr. [a], Takumi Takashima [a], Takashi Oozeki [a], Ken-ichi Shimose [b], Yoshinori Yamada [c]

[a] Research Center for Photovoltaic Technologies, National Institute of Advanced Industrial Science and Technology, Tsukuba, Japan
[b] Department of Monitoring and Forecasting Research, National Research Institute for Earth Science and Disaster Prevention, Tsukuba, Japan
[c] Meteorological Research Institute, Japan Meteorological Agency, Tsukuba, Japan

Received 13 March 2014; received in revised form 5 February 2015; accepted 11 March 2015
Available online 13 April 2015

Communicated by: Associate Editor Christian A. Gueymard

Abstract

To obtain accurate forecasts of photovoltaic power generation, the use of forecast datasets of meteorological elements from numerical prediction models, specifically global horizontal irradiance (GHI), is necessary. This study seeks to validate, and therefore improve GHI forecasts. Ground-based data from Japan Meteorological Agency (JMA) stations are used in a JMA mesoscale model (MSM) during the time period from 2008 to 2012 and temporal and spatial characteristics of forecast errors are analyzed. Statistical monthly evaluations show that associated errors vary between seasons, with monthly GHI mean bias error values ranging from −60 to +45 W/m^2 and root mean square errors (RMSEs) ranging from 95 to 170 W/m^2. Mapping of forecast errors show that underestimation of GHI forecast values and large RMSE values are significant in the southern part of Japan (a subtropical region located along the Pacific Ocean), particularly during summers. In winter, overestimation of GHI forecasts is found throughout the entire Japanese archipelago. The frequency of different cloud type occurrences over the Japanese islands indicate that regional and seasonal variations in cloud types are related to relatively large GHI forecast errors. High-level cirrus clouds, mid-level altocumulus, and low-level stratus are often observed during summer, when forecasted values are underestimated, and during winter, when values are overestimated.

Keywords: Mesoscale model; GHI; Forecast errors; Japanese islands

1. Introduction

Obtaining an energy supply from renewable sources is desirable for two important reasons: to match ever-increasing energy demands without relying on limited fossil fuel sources and to ameliorate the effects of climate change by decreasing carbon dioxide. Achieving these goals in Japan is important, and this makes the use of renewable sources vital in the management of power generation. In this scenario, photovoltaic (PV) power generation is expected to become an important source of renewable energy in Japan. As such, a PV energy source is strongly dependent on solar radiation (i.e., global horizontal irradiance; GHI), and its proper forecast and assessment have a fundamental role in PV power generation.

* Corresponding author at: Research Center for Photovoltaic Technologies, National Institute of Advanced Industrial Science and Technology, OSL, Tsukuba Central 2, 1-1-1 Umezono, Tsukuba, Ibaraki 305-8568, Japan. Tel.: +81 29 849 1526; fax: +81 29 861 5829.
E-mail address: hideaki-ootake@aist.go.jp (H. Ohtake).

http://dx.doi.org/10.1016/j.solener.2015.03.020
0038-092X/

PV power generation forecasts have been performed based on engineering techniques using meteorological forecast datasets (e.g., Fonseca et al., 2011). However, overall forecast accuracy is dependent on the forecast accuracy of each meteorological element, including GHI.

Moreover, large variations in PV power generation are mainly caused by variations in meteorological elements such as cloud cover and aerosols. Thus, it is clear that the production of a large amount of renewable energy in Japan is significantly dependent on the weather; therefore gaining an understanding of the characteristics of GHI forecast errors is important in the operation and integration of such systems in current power grids.

Output data from a numerical weather prediction model (NWP) has been considered useful in forecasting PV power generation and in energy management planning. The Japan Meteorological Agency (JMA) developed a mesoscale non-hydrostatic model (NHM, Saito et al., 2006, 2007) to use as an operational forecast model. Recently, many researchers and private-sector corporations in Japan have used grid point values from this model to develop PV power forecasts. GHI forecasts are also yielded by the model and can become very useful in PV power forecasts. However, GHI forecasts obtained from the NWP invariably contain errors. Therefore, in order to improve the MSM results it is necessary to first understand the characteristics of GHI forecast errors.

Intra-day solar irradiance (i.e., the downward shortwave component of radiation processes) forecasts obtained from different NWPs (e.g., Mathiesen and Kleissl, 2011) and regional GHI forecast error characteristics have been evaluated in previous studies (e.g., Zamora et al., 2005; Perez et al., 2010; Davy and Troccoli, 2011; and Pelland et al., 2011). Davy and Troccoli (2011) investigated seasonal GHI productivity and the relationship between regional forecast errors and climatic phenomena.

In addition, errors in forecasted regionally averaged GHI values throughout all the Japanese islands have been verified and have continuously improved. For example, Nagasawa (2008) investigated the mean bias errors (MBE) and root mean square errors (RMSE) in GHI forecasts using surface GHI values measured at 65 JMA stations over a four-year period between 2004 to 2007. Statistical evaluations showed significant negative bias in the GHI values and large monthly RMSE values (about 200 W/m^2), particularly during the summer. Yoshida et al. (2011) also verified GHI forecast errors using the NHM in the Tohoku region (northeastern Japan) and reported overestimated values during the summer. Ohtake et al. (2013a) examined errors in the MSM GHI forecasts using surface GHI observations from JMA stations in a specific region (i.e., Kanto region, central Japan) and found negative (positive) biases in the summer (winter) seasons.

In spite of these studies, regional variability in MSM GHI forecasts have not been addressed in the literature. Therefore, the present study analyzes the characteristics of both spatial and temporal (e.g., monthly, seasonal, and annual) errors characteristics in MSM GHI forecasts, and observed weather conditions.

In Section 2 of this paper, both the surface-measured JMA GHI dataset and the setting of the MSM analyzed in this study are described in detail. Annual and seasonal GHI forecast errors are analyzed in Section 3. Section 4 presents regional forecast error characteristics and analyzes the relationship between the errors and weather conditions (i.e., cloud types). Finally, Section 5 summarizes and discusses the findings of this study.

2. Data

2.1. Observational data

Pyranometers (Kipp & Zonen CM 3, CM 21, CMP 22, and EKO MS 62) were used to measure surface GHI from 2008 to 2011 at 47 JMA stations (see Table 1). In the middle of 2011, most of the pyranometers installed were replaced with EKO MS 402 units. In addition, the number of JMA stations measuring GHI decreased from 52 in January 2008 to 48 in December 2012. Five JMA stations, Sapporo (1), Tsukuba (47), Fukuoka (31), Ishigajikijima (42) and Minami-Torishima (Table 1), are Baseline Surface Radiation Network (BSRN) stations. Direct and diffuse solar irradiance are separately observed at these stations. Minami-Torishima JMA station (located at 153.98°E, 24.29°N) was removed from analysis because it was located outside of the MSM domain. Diffuse solar irradiance from direct sunlight was measured using a pyranometer with an automatic sun-tracking shadowing disk (to avoid direct solar irradiance).

The JMA performed quality control of all the measured GHI data. Maintenance of the GHI measurements is an important factor for the quality of the GHI observations. The glass domes of the measurements were routinely cleaned using a feather brush and a soft cloth (at least one a weak) to remove contaminants such as dust, ice and snow particles which can significantly affect the measurement by JMA operational staffs. Each pyranometer sampled GHI values at intervals of 10 s, and 1 min averages were calculated from the sampled data. Furthermore, in order to validate the MSM GHI forecasts, hourly-averaged GHI values were calculated using observed data.

2.2. Numerical model

Forecasted GHI values were calculated at each station using the MSM (the operational model in Japan developed from the non-hydrostatic model, e.g., Saito et al., 2006, 2007). The model was initialized using the same specifications as those described by Ohtake et al. (2013a). The model domain included a region surrounding the Japanese Island $3600 \times 2900 \times 21.8$ km in size along the x, y, and z axes, respectively, with a horizontal grid spacing

Table 1
Instruments (pyranometers and pyrheliometers) and the period of installation at JMA stations. The location of each station is shown in Fig. 1. The term "diffuse" indicates diffuse irradiances, which are measured from direct sunlight using a pyranometer. A diffuse sensor is shaded by an automatic sun-tracking shadowing disk in order to avoid direct solar irradiance.

Number	Station	Period 1 -03/2010	Period 2 03/2010-	
		GHI	Direct	Diffuse
1	Sapporo	CM 21	CHP 1	CMP 22
31	Fukuoka	CM 21	CHP 1	CMP 22
42	Ishigakijima	CM 21	CHP 1	CMP 22

Number	Station	Period 1 -07/2011		Period 2 08/2011-	
		Pyrheliometer	Diffuse	Pyrheliometer	Diffuse
47	Tsukuba	CH 1	CM 21	CHP 1	CMP 22

Number	Station	Period 1	Period 2	Number	Station	Period 1	Period 2
2	Wakkanai	MS 62 -06/2011	MS 402 07/2011-	24	Osaka	MS 62 -02/2011	MS 402 03/2011-
3	Abashiri	MS 62 -07/2011	MS 402 08/2011-	25	Nara	MS 62 -11/2012	MS 402 12/2012-
4	Asahikawa	MS 62 -06/2011	MS 402 07/2011-	26	Hikone	MS 62 -02/2011	MS 402 03/2011-
5	Obihiro	MS 62 -09/2011	MS 402 10/2011-	27	Hiroshima	MS 62 -02/2011	MS 402 03/2012-
6	Muroran	MS 62 -05/2011	MS 402 06/2011-	28	Takamatsu	MS 62 -11/2011	MS 402 12/2011-
7	Sendai	CM 3 -02/2011	MS 402 03/2011-	29	Matsuyama	MS 62 -12/2011	MS 402 01/2012-
8	Aomori	CM 3 -06/2011	MS 402 07/2011-	30	Kochi	MS 62 -11/2012	MS 402 12/2012-
10	Morioka	CM 3 -07/2011	MS 402 08/2011-	32	Shimonoseki	CM 3 -11/2011	MS 402 12/2011-
11	Yamagata	CM 3 -07/2011	MS 402 08/2011-	33	Oita	CM 3 -11/2012	MS 402 12/2012-
12	Fukushima	CM 3 -08/2011	MS 402 09/2011-	34	Saga	CM 3 -12/2012	MS 402 01/2013-
13	Tokyo	CM 3 -06/2011	MS 402 07/2011-	35	Kumamoto	CM 3 -10/2012	MS 402 11/2012-
14	Utsunomiya	CM 3 -02/2011	MS 402 03/2011-	37	Naze	CM 3 -12/2012	MS 402 01/2013-
15	Maebashi	CM 3 -11/2011	MS 402 12/2011-	38	Miyazaki	CM 3 -10/2012	MS 402 11/2012-
16	Choshi	CM 3 -02/2011	MS 402 03/2011-	39	Okinawa	CM 21 -02/2011	MS 402 03/2011-
17	Nagano	CM 3 -02/2011	MS 402 03/2011-	40	Minamidaitou-jima	MS 62 -11/2013	MS 402 12/2013-
18	Kofu	CM 3 -02/2011	MS 402 03/2011-	41	Miyakojima	MS 62 -01/2014	MS 402 02/2014-
19	Nagoya	CM 3 -02/2011	MS 402 03/2011-	43	Hakodate	MS 62 -06/2011	MS 402 07/2011-
20	Shizuoka	CM 3 -02/2011	MS 402 03/2011-	44	Nagasaki	CM 3 -11/2012	MS 402 12/2012-
21	Niigata	CM 3 -05/2012	MS 402 06/2012-	45	Maizuru	MS 62 -09/2012	MS 402 10/2012-
22	Toyama	CM 3 -02/2011	MS 402 03/2011-	46	Chichijima	MS 62 -01/2012	MS 402 02/2012-
23	Fukui	CM 3 -04/2011	MS 402 05/2011-				

Number	Station	Period 1	Period 2	Period 3
9	Akita	CM 21 -11/2010	CM 3 12/2010 -04/2011	MS 402 05/2011-
36	Kagoshima	CM 21 -01/2011	CM 3 02/2011 -12/2012	MS 402 01/2013-

of 5 km and a 24 s time step. Radiative transfer processes were calculated by thinning out every other grid point in the x and y directions. The horizontal spatial resolution of MSM GHI forecasts was 10 km. However, it is difficult to unambiguously represent variations in solar irradiance on spatial scales smaller than 40 km. Solar irradiance was calculated at 15-min intervals. GHI forecasts were averaged every hour, then archived.

A three-ice bulk microphysics scheme that considers the fall speed of cloud ice and one-moment parameterizations (Ikawa and Saito, 1991) was applied to the MSM, along with the Kain-Frisch cumulus parameterization (Kain and Fritsch, 1993). In the MSM, a renewed version of the original Kain-Frisch cumulus parameterization improved by Ohmori and Yamada (2004) are introduced.

The model initial conditions were provided by a four-dimensional variational data assimilation technique (Meso 4DVAR, Ishikawa and Koizumi, 2002). New periodic and/or non-periodical observational data were assimilated in space and time into a previous model forecast, and this output was used to initialize a subsequent model run. The lateral boundary conditions were supplied by the JMA global spectral model with a horizontal grid spacing of 20 km and a 6-h time intervals.

Each day, the model was started at 3-h intervals (8 times per day), producing 15-h and 33-h forecasts of GHI values. The relatively longer forecast outputs (33-h) were initialized at 03 h, 09 h, 15 h, and 21 h UTC (Universal Coordinated Time), or 12 h, 18 h, 00 h, and 06 h LST (Local Standard Time, i.e., UTC + 9 h). Noted that the 15 h and 21 h UTC initialization times correspond to 00 h and 06 h LST the following day.

The 22-band model was used for the MSM shortwave radiative scheme, and was based on parameterizations of optical absorption of water vapor (Briegleb, 1992) and other gases (Freidenreich and Ramaswamy, 1999). Cloud

optical parameters (e.g., optical thickness, single scattering albedo, and asymmetry factor) were estimated from vertically integrated water or ice content (based on Slingo (1989) for water clouds and Ebert and Curry (1992) for ice clouds). The effective radii of cloud ice particles, which were determined by an equation dependent only on temperature, were calculated following Ou and Liou (1995). The time interval of the radiative transfer calculations was fixed as 15 min, and the analyses were made using five-year data recorded from 2008 to 2012.

2.3. Error evaluation

Forecast errors were assessed using MBE and RMSE, which are defined as

$$\mathrm{MBE} = \frac{1}{N}\sum_{i=1}^{N}(\mathrm{FCST}_i - \mathrm{OBS}_i) \tag{1}$$

$$\mathrm{RMSE} = \sqrt{\frac{1}{N}\sum\nolimits_{i=1}^{N}(\mathrm{FCST}_i - \mathrm{OBS}_i)^2} \tag{2}$$

where FCST and OBS are the MSM GHI forecasts and surface-measured GHI values, respectively, and N is the total number of samples. Relative forecast errors (rMBE and rRMSE) were also calculated every hour using the GHI observations in order to remove seasonal and daily variations in solar irradiance (i.e., solar altitude) and are defined as

$$\mathrm{rMBE} = \frac{1}{N}\sum_{i=1}^{N}\frac{(\mathrm{FCST}_i - \mathrm{OBS}_i)}{\mathrm{OBS}_i} \tag{3}$$

$$\mathrm{rRMSE} = \sqrt{\frac{1}{N}\sum\nolimits_{i=1}^{N}\left(\frac{\mathrm{FCST}_i - \mathrm{OBS}_i}{\mathrm{OBS}_i}\right)^2} \tag{4}$$

Forecasts obtained from the 21 h UTC initialization time (06 h LST on the following day) were produced from 07 h LST. Although GHI forecasts were evaluated throughout the period 07 h LST to 21 h LST, only data recorded during daylight hours (i.e., positive values of extraterrestrial solar irradiance) were used in this evaluation (night time data are excluded). This procedure was adopted to analyze the MSM performance for solar irradiance during daylight hours. That is, all solar zenith angles less than 89.9 degrees.

3. Annual and seasonal variations in GHI forecast errors

In this section, annual and seasonal variations in GHI forecast errors are analyzed for the entire area encompassing the Japanese islands. Fig. 1a shows a time series of MBE for forecasted monthly GHI from January to December 2012 based on surface-measured GHI from 47 stations. It was found that forecasted GHI values from late autumn to spring (November through April) tended to be overestimated but that significant underestimations in forecasted GHI values were found during the summer (July and August). Monthly MBE values ranging from −60 to +45 W/m^2 were found, and similar tendencies were consistently seen from 2008 to 2012. There were no apparent large differences each month in the MBE values for the four

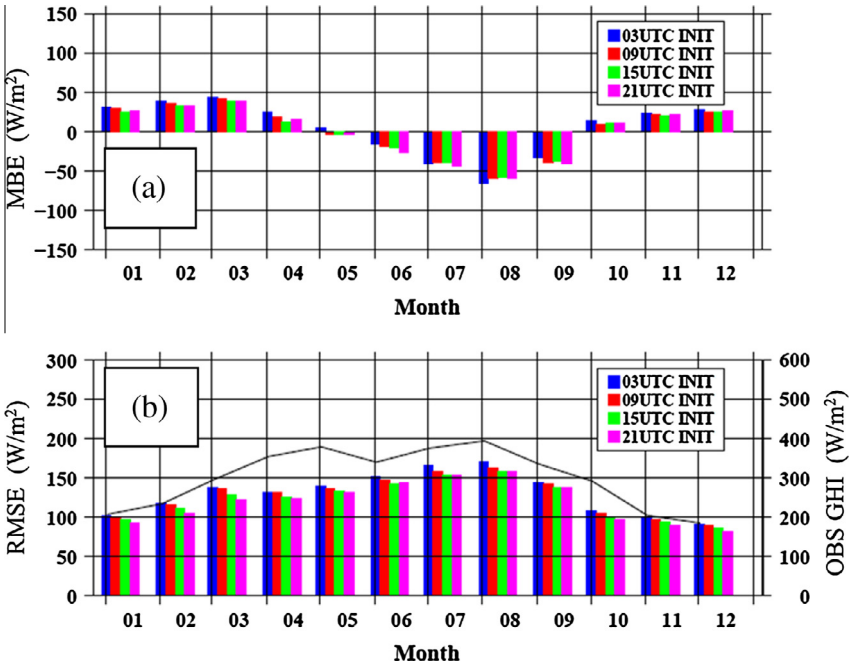

Fig. 1. Time series of monthly (a) mean bias error (MBE; W/m^2), and (b) root mean square error (left vertical axis, RMSE; W/m^2) of GHI values for all surface stations (a total of 47 stations) during the year 2012. The blue, red, green and pink columns indicate results using different initialization times of 03 h, 09 h, 15 h and 21 h UTC, respectively. Solid line in (b) shows monthly-averaged GHI observations (right vertical axis; W/m^2).

Table 2
Statistical evaluations of annual GHI values for the five years from 2008 to 2012 and seasonal GHI values during winter (DJF), spring (MAM), summer (JJA) and autumn (SON), with different initialization times (03 h, 09 h, 15 h and 21 h UTC) and observations (OBS) for all JMA stations. MBE and RMSE are measured in W/m^2. Seasons are defined as follow; winter (December–February or DJF), spring (March–May or MAM), summer (June–August or JJA), and autumn (September–November or SON).

Initial time	2008		2009		2010		2011		2012	
	MBE (W/m^2)	RMSE (W/m^2)	MBE (W/m^2)	RMSE (W/m^2)	MBE (W/m^2)	RMSE (W/m^2)	MBE (W/m^2)	RMSE (W/m^2)	MBE (W/m^2)	RMSE (W/m^2)
Annual										
OBS		313.1		311.8		309.0		309.5		306.8
03UTC	3.8	138.6	−2.0	136.3	−1.9	136.9	−4.7	139.8	1.7	138.5
09UTC	0.2	136.7	−4.3	133.5	−4.3	134.3	−6.0	135.7	−0.9	135.0
15UTC	−3.9	131.4	−5.2	129.4	−5.4	129.5	−6.8	131.5	−2.4	130.0
21UTC	−2.6	129.7	−4.0	125.6	−2.5	123.8	−6.4	126.0	−2.1	124.6
Winter (DJF)										
OBS		226.2		221.0		220.2		228.2		209.9
03UTC	19.9	101.7	24.1	105.2	25.7	100.7	23.4	104.8	33.3	104.4
09UTC	15.1	100.0	21.5	103.2	25.5	100.8	21.7	102.9	30.2	102.8
15UTC	14.3	94.8	20.4	100.0	24.7	97.5	21.2	99.1	28.0	98.6
21UTC	12.4	95.6	19.6	98.6	25.3	95.2	22.1	97.0	28.4	94.1
Spring (MAM)										
OBS		357.4		372.2		333.6		352.9		343.9
03UTC	35.3	145.7	3.6	139.6	16.9	145.5	17.1	142.1	24.9	140.5
09UTC	30.6	143.4	2.7	136.8	14.6	140.9	14.2	139.1	19.4	138.8
15UTC	23.6	135.2	2.5	132.0	11.1	134.6	12.6	134.5	16.0	132.7
21UTC	25.8	132.5	2.3	127.0	12.8	127.9	12.0	128.1	17.1	126.4
Summer (JJA)										
OBS		371.3		349.0		377.7		365.8		370.4
03UTC	−34.8	170.0	−30.9	166.1	−41.1	162.5	−50.5	175.6	−43.5	170.2
09UTC	−39.6	169.5	−33.8	162.7	−44.5	160.6	−50.6	169.1	−42.5	163.5
15UTC	−41.1	165.1	−34.5	157.9	−45.5	155.2	−49.5	164.9	−42.8	158.2
21UTC	−34.6	162.3	−29.5	154.3	−39.7	148.4	−48.6	157.3	−43.1	151.9
Autumn (SON)										
OBS		276.7		282.6		278.6		269.2		280.6
03UTC	−1.1	118.0	1.9	117.6	−1.3	120.3	−1.4	116.1	−0.1	121.5
09UTC	−1.0	114.3	−1.1	115.5	−4.6	117.6	−1.8	112.8	−3.8	119.2
15UTC	−8.0	110.5	−2.7	112.0	−3.5	114.1	−4.2	108.3	−3.7	115.0
21UTC	−10.5	109.7	−2.8	107.2	−0.7	108.5	−3.7	104.2	−4.0	111.4

different initialization times of 03 h, 09 h, 15 h and 21 h UTC.

The time series of GHI RMSE values also showed critical seasonal variations with relatively large (small) RMSE in summer (winter) (Fig. 1b). RMSE values from autumn to winter decreased to about 90 W/m^2 (in December) but from spring to summer increased to about 170 W/m^2. A comparison of RMSE values using different initialization times, from 03 h UTC on the previous day (12 h LST on the same day) to 21 h UTC on the previous day (06 h LST on the target day), revealed a relatively large difference in RMSE during the summer (about 10 W/m^2) compared to other seasons.

The various initialization times had different lead times. In this analysis, for example, 03 h UTC forecasts on the day before (12 h LST on the day before) correspond to a one day forecast. Forecasts at 21 h UTC on the previous day (06 h LST on the target day) are considered to be a same-day forecast. Therefore, the lead-time of 21 h UTC forecasts was shorter than those of 03 h, 09 h and 15 h UTC forecasts. It is considered that 21 h UTC initialization forecasts (to which up-to-date observational datasets are assimilated) tended to deliver smaller forecast errors than forecasts using other initialization times. In addition, monthly-averaged GHI observed values are added in Fig. 1b. Temporary decrease of solar irradiance are found during early summer season because of a rainy season around the Japan islands in the period from June to mid-July.

Annual and seasonal changes in the GHI forecast errors (MBE and RMSE) at JMA stations are presented in Table 2. Annual MBE values with different initialization times ranged from −6.8 to +3.8 W/m^2 throughout the four-year dataset. RMSE values ranged from 136.3 to 139.8 W/m^2 for the forecasts initialized at 03 h UTC and 123.8 to 129.7 W/m^2 for values from 21 h UTC forecasts.

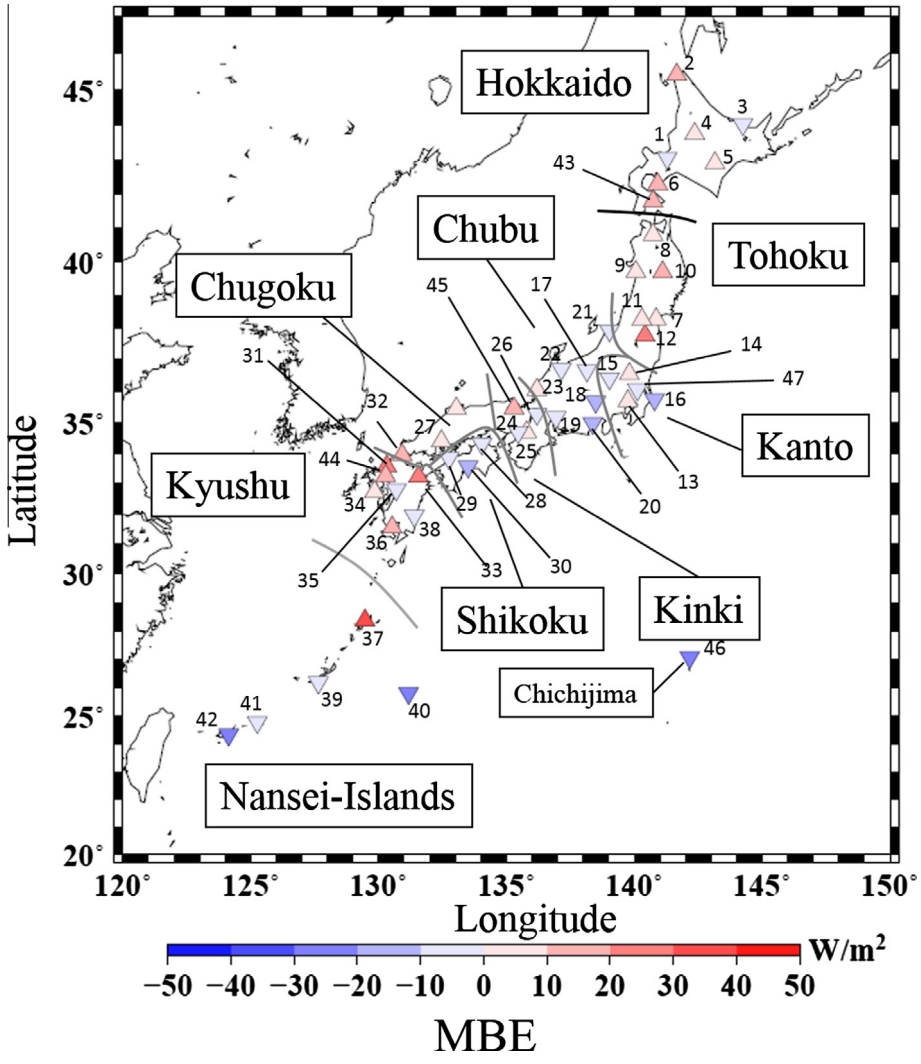

Fig. 2. Map of annual GHI MBE values for the initialization time of 03 h UTC during 2012 in Japan. Each number indicates the JMA station at which GHI was observed (see Table 1).

The difference between RMSE values is therefore low (a maximum of 16.0 W/m^2). As the forecast lead-time was reduced from 03 h UTC to 21 h UTC initialization times, the forecast error values tended to become smaller each year. As the lead-time became shorter, the most up-to-date observational datasets that represent actual atmospheric conditions were inserted into the model. There was almost no observable annual tendency in the RMSE values during the years from 2008 to 2012.

As a reference data, we added annual and seasonal averaged GHI observation values (OBS shown in Table 2) calculated. Mean observed values are almost the same (around approximately 310 W/m^2) during the years from 2008 to 2012. Maximum difference of mean observed GHI values for summer seasons is 28.7 W/m^2 between 2009 and 2010.

For the seasonal analysis, an overestimation in GHI forecasts (a positive MBE) was found during the winter (December, January, and February or DJF) and spring seasons (March, April, and May or MAM). On the other hand, an underestimation (negative MBE) occurred during the summer (June, July, and August or JJA). RMSE values in summer during 2008 and 2011 were relatively large compared with those in 2009 and 2010. MBE values during the autumn (September, October, and November or SON) showed a weak underestimation of GHI.

4. Mapping of GHI forecast errors

4.1. Annual averaged forecast errors and regional characteristics

Japan was the target area of analysis in this paper (shown in Fig. 2). The country has a length of approximately 3,000 km and is oriented northeast to southwest (approximately 45°N, 145°E to 25°N, 125°E). A mountainous region (relative high topography, ~3000 m) prevails over central Japan, and the country has a variety of climatic regions. The Hokkaido islands in the northern part of Japan are in a subarctic climate. The region from

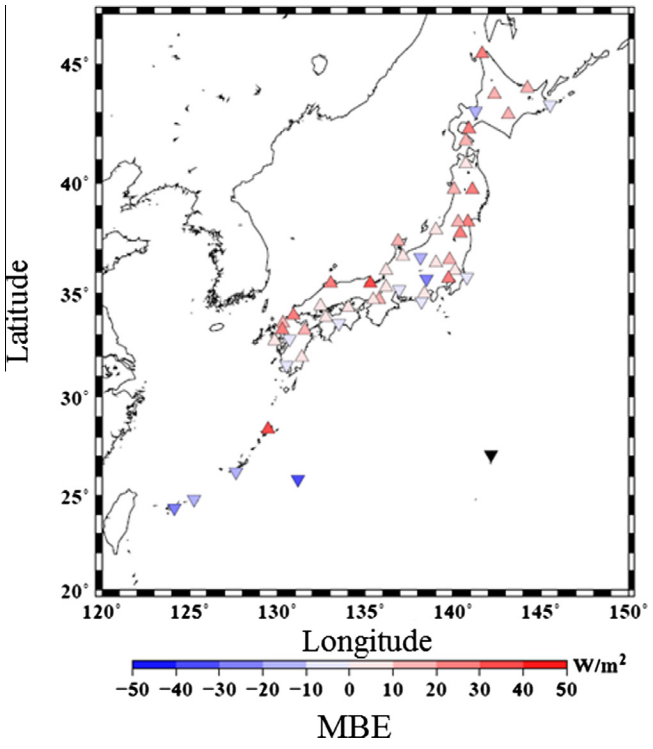

Fig. 3. Same as Fig. 2, but during 2008.

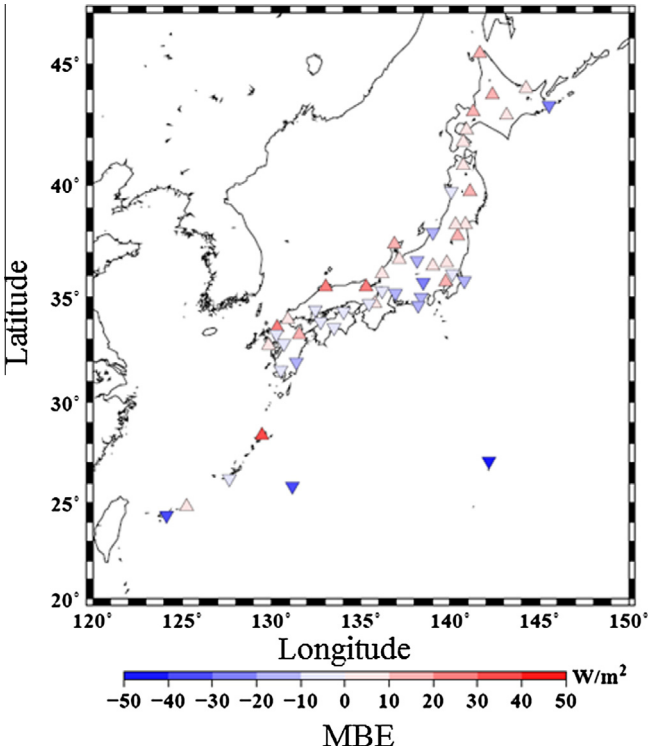

Fig. 4. Same as Fig. 2, but during 2009.

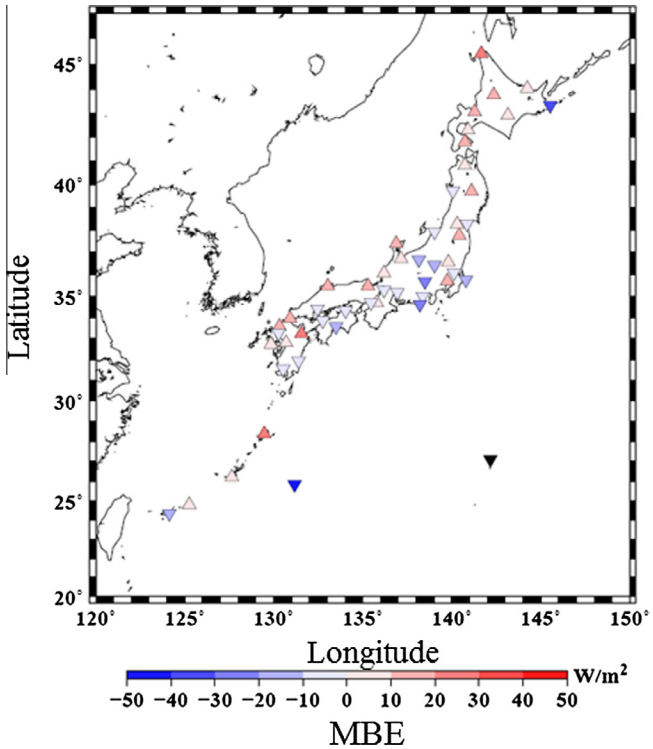

Fig. 5. Same as Fig. 2, but during 2010.

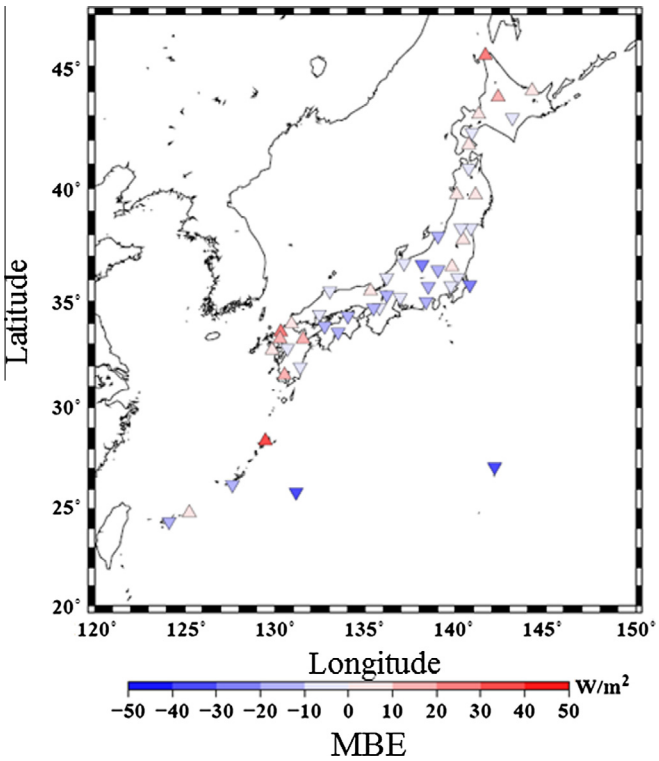

Fig. 6. Same as Fig. 2, but during 2011.

Tohoku to Kyushu is in a generally humid and temperate climate. In the winter, there is considerable snowfall in the coastal regions along the Sea of Japan, from Hokkaido to Kyushu. A subtropical climate dominates in the southwestern part of Japan and total precipitation is larger here than in other regions. Saito et al. (2006) described the non-hydrostatic model (NHM, the same as our operational model) and investigated its performance

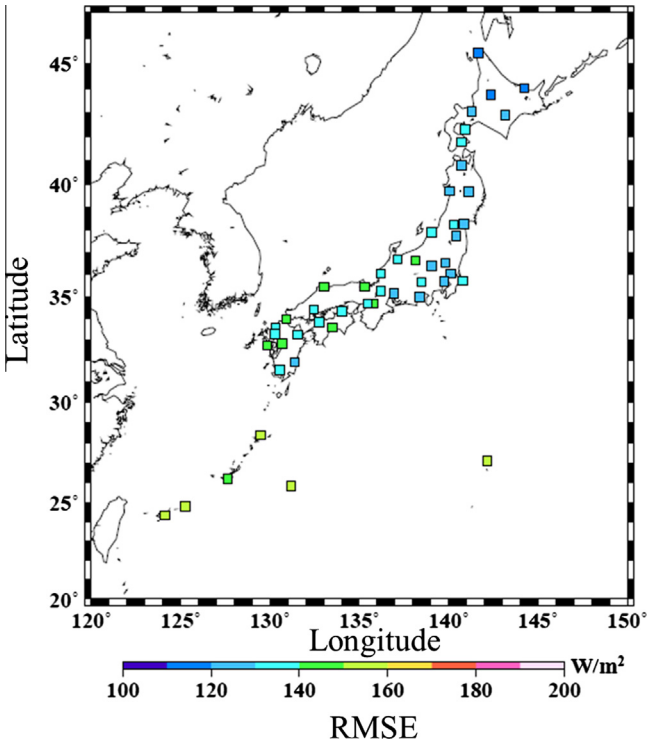

Fig. 7. Map of annual GHI RMSE values in Japan during 2012 for an initialization time of 03 h UTC.

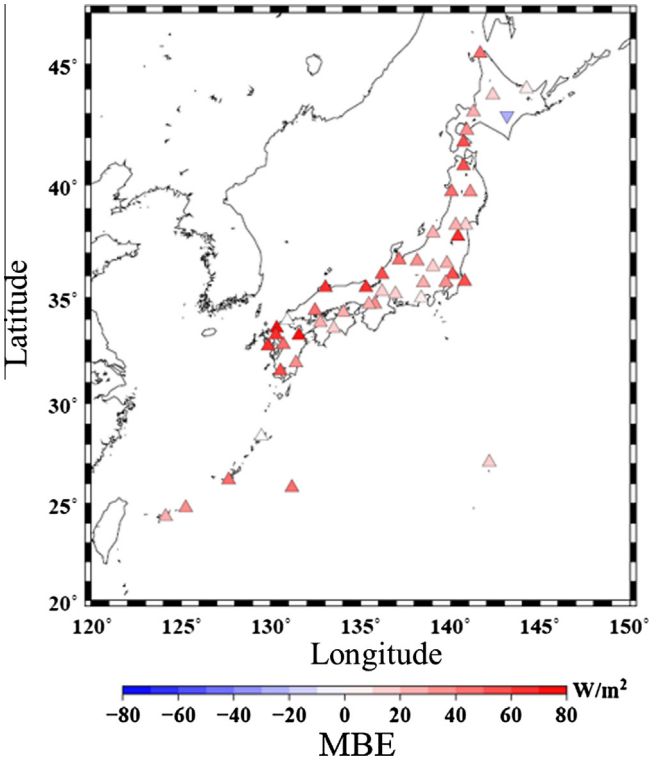

Fig. 8. Map of seasonal GHI MBE values during winter (DJF) 2012 for an initialization time of 03 h UTC. Red triangles and blue inverted triangles indicate positive and negative bias errors, respectively. (For interpretation of the references to colour in this figure legend, the reader is referred to the web version of this article.)

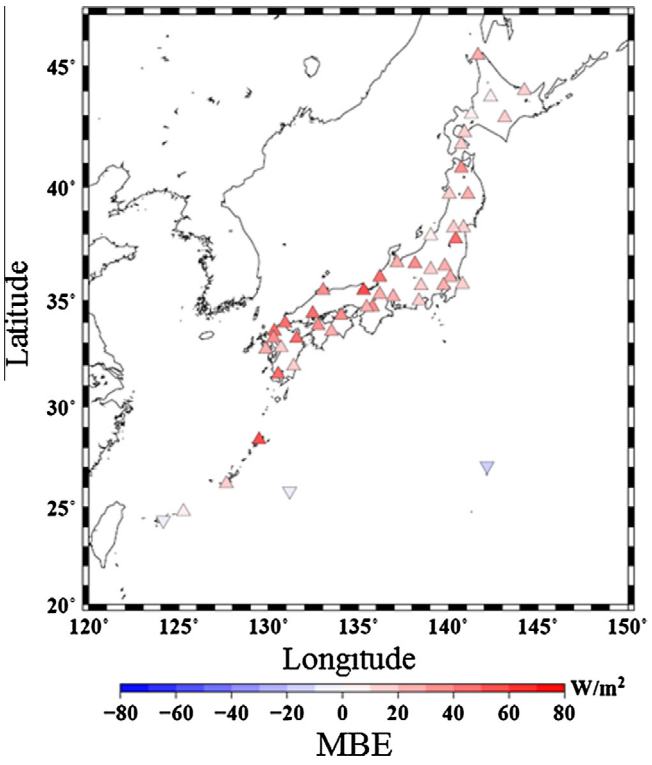

Fig. 9. Same as Fig. 8, but during spring (MAM).

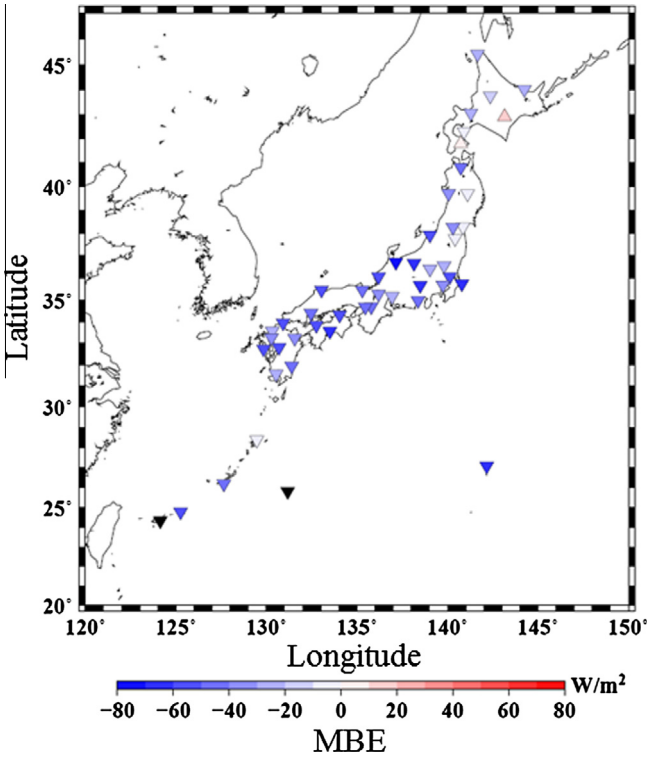

Fig. 10. Same as Fig. 8, but during summer (JJA).

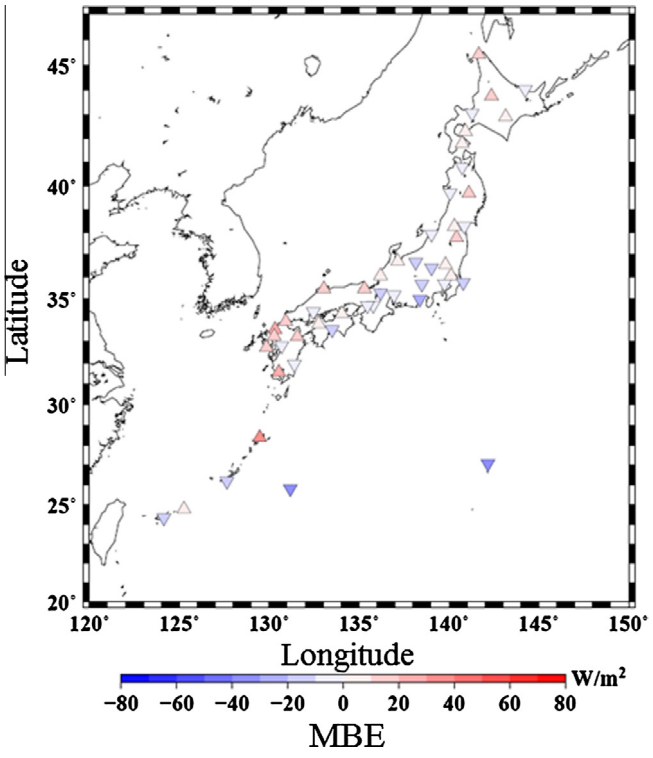

Fig. 11. Same as Fig. 8, but during autumn (SON).

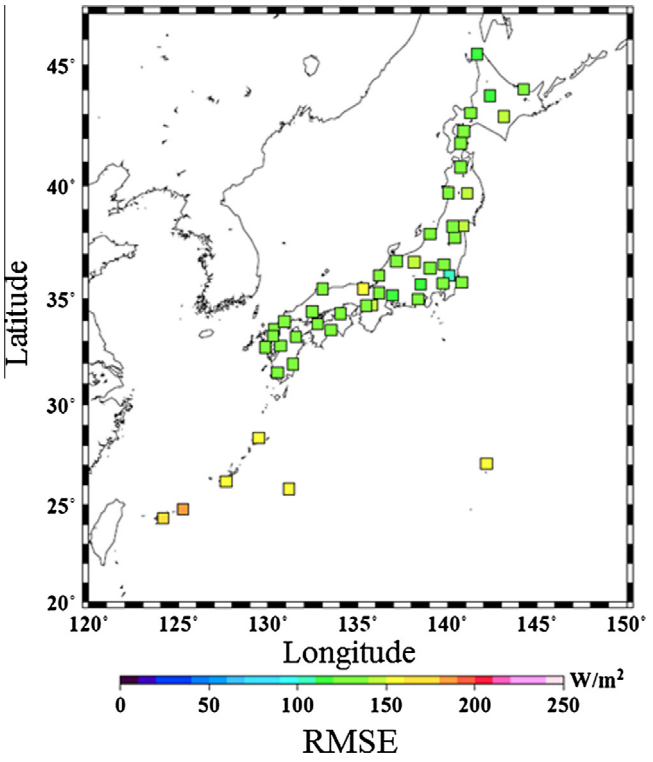

Fig. 13. Same as Fig. 12, but during spring (MAM).

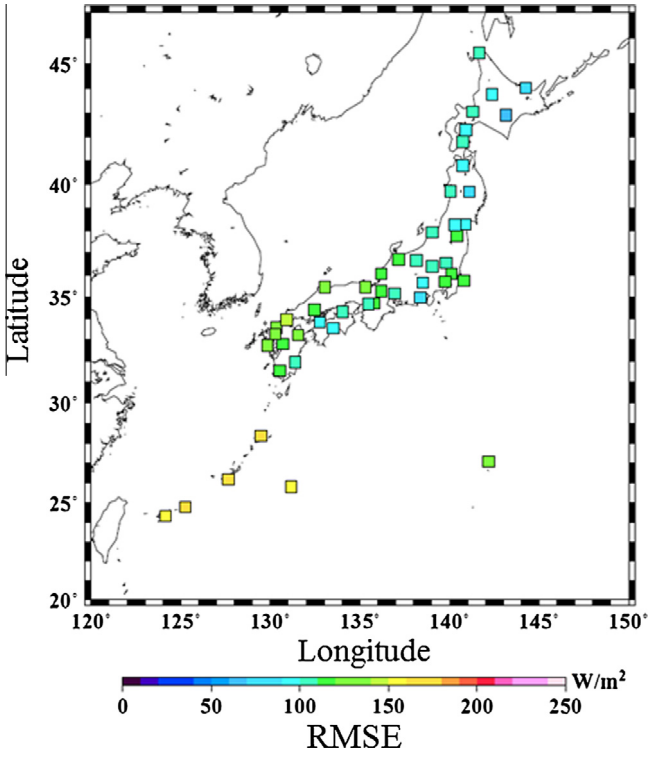

Fig. 12. Map of seasonal GHI RMSE values during winter (DJF) 2012.

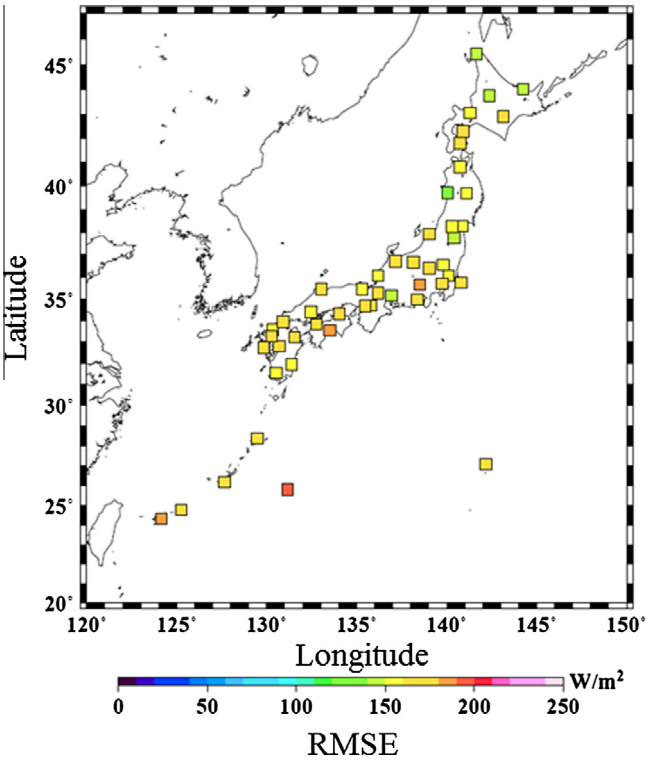

Fig. 14. Same as Fig. 12, but during summer (JJA).

based on case studies that included several meteorological events (i.e., a winter monsoon cold-air outbreak and a typhoon).

To understand the regional characteristics of GHI forecast errors, annual MBE values during 2012 have been mapped (Fig. 2). The GHI forecast errors at each station

show underestimations in regions lying near the coast along the Pacific Ocean (from the Kanto region to the Shikoku region) but not in the Hokkaido (northern Japan) and Kyushu regions (western Japan). In particular, we found a significant underestimation at some stations in the Nansei-Islands (the southwestern part of Japan) and at the Chichijima station, all of which are located in a subtropical climate. A comparison of the results from the other four years (from 2008 to 2011, Figs. 3–6) showed that the local and/or regional MBE variations were different each year. Absolute magnitudes of GHI forecast errors are almost the same, whereas negative and positive values are appeared year by year. In particular, there were a large number of positive biases in 2008 (Fig. 3) and negative biases in 2011 (Fig. 6). However, ranges of the forecast errors were nearly the same during all years.

Fig. 7 shows a map of annually averaged GHI forecast RMSE values during 2012. Values ranging from 100 to 140 W/m^2 for most of the areas from northern Japan to the Kyushu region, whereas values in the Nansei-Islands reached about 160 W/m^2. In general, RMSE values in the southern part of Japan, which is classified as a subtropical climate, were relatively large compared to those in the mid-latitude regions. However, the annual changes in these regional characteristics during the period from 2008 to 2012 were not significantly large.

4.2. Seasonal changes

To understand the seasonal changes in GHI forecast errors, we performed a regional mapping of seasonal MBE values during 2012 (shown in Figs. 8–11). From winter (DJF) to spring (MAM) (see Figs. 8 and 9), the GHI values were significantly overestimated throughout the entire country, except in several inland stations. However, GHI forecasts over the sea off the south coast of Japan were underestimated. During summer (JJA, Fig. 10), there was a significant underestimation of GHI values over most of the Japanese Islands. In autumn (Fig. 11), MBE values and ranges of values decreased. In addition, no large annual differences in seasonal MBE values were found between 2008 to 2012 (not shown).

Maps of RMSE values for each season in 2012 are also shown in Figs. 12–15. Note that the scale of the color bar is different from that in Fig. 7 due to relatively large seasonal variations in the RMSE values at each station. During winters (DJF, Fig. 12), some regional RMSE values between northern Japan and the Shikoku islands were less than 100 W/m^2. However, differences at each station tended to be small. At stations in the western part of Japan (from Chugoku to Kyushu), the RMSE values were larger than 100 W/m^2. In addition, at stations on the Nansei-islands, the RMSE values were larger than 150 W/m^2. During spring (MAM, Fig. 13), there was an overall increase in RMSE values throughout the entire country. RMSE values in the southern part of Japan (<30°N in latitude) were larger than 150 W/m^2. During summer (i.e., the rainy

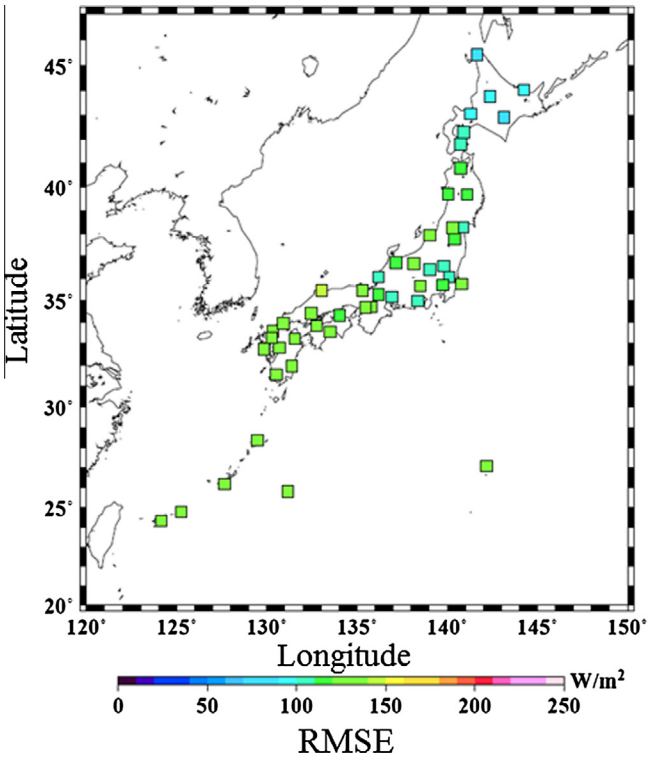

Fig. 15. Same as Fig. 12, but during autumn (SON).

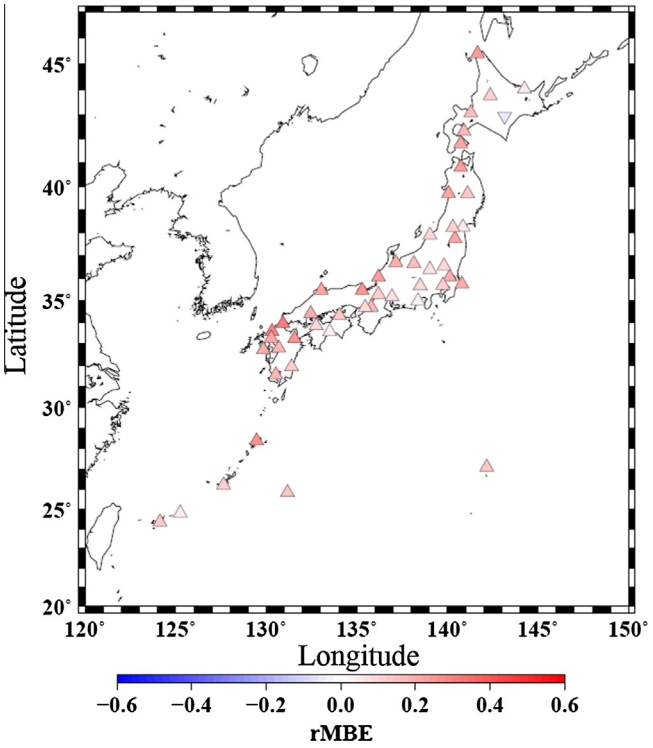

Fig. 16. Map of seasonal GHI rMBE values during winter (DJF) 2012 with an initialization time of 03 h UTC. Red triangles and blue inverted triangles indicate positive and negative bias errors, respectively. (For interpretation of the references to colour in this figure legend, the reader is referred to the web version of this article.)

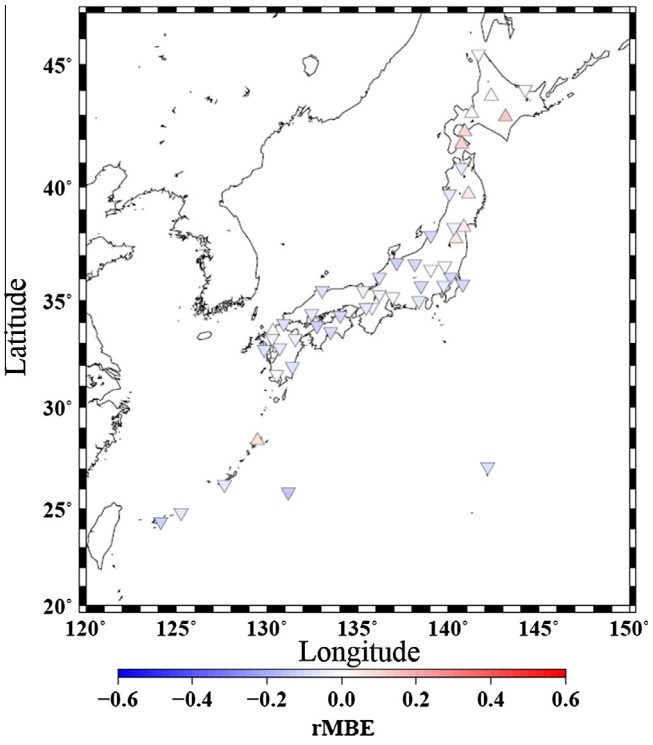

Fig. 17. Same as Fig. 16, but during summer (JJA).

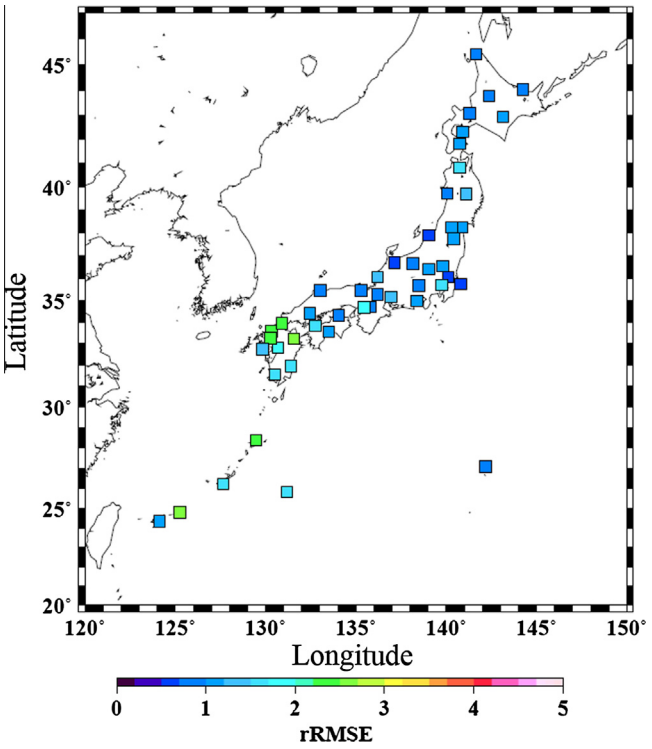

Fig. 19. Same as Fig. 18, but during summer (JJA).

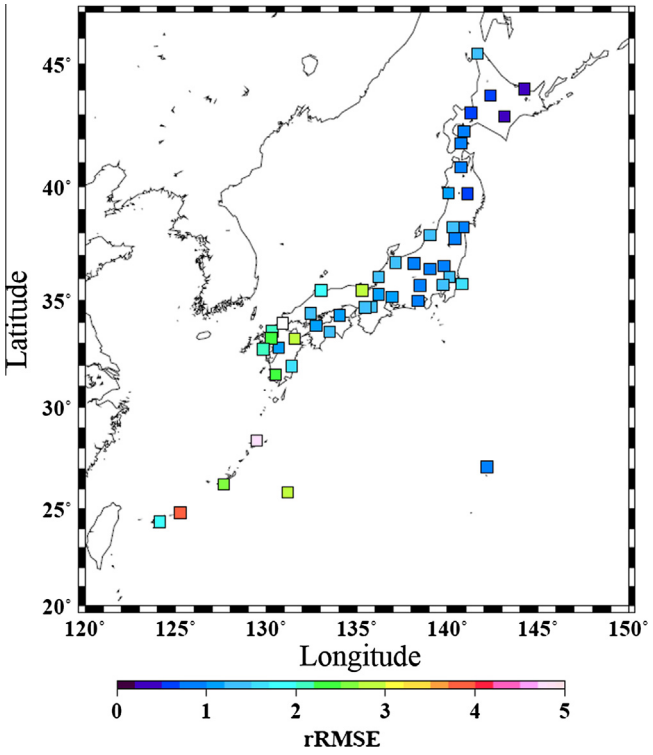

Fig. 18. Map of seasonal GHI rRMSE values during winter (DJF) 2012 with an initialization time of 03 h UTC.

season in the Japan islands) these values became generally large (Fig. 14), although regional differences were found. From summer (JJA, Fig. 14) to autumn (SON, Fig. 15) RMSE values decreased gradually in Japan, and regional distributions of RMSE in both spring and autumn seasons were similar. The pattern of RMSE distributions from 2008 to 2011 was also similar to those in 2012 (not shown).

GHI values at the surface are dependent on solar altitude. Therefore, in order to gain an understanding of MSM forecast errors, we calculated relative forecast errors and normalized values using surface-observed solar irradiance. Figs. 16 and 17 show maps of the relative MBE (shown as "rMBE" in the figures) during winter and summer of 2012, respectively. During winter, rMBE values at each station showed almost the same positive tendency (Fig. 16), and in the western part of the main islands of Japan relatively large positive values were also found. During the summer, the same level of negative rMBE (about 0.1) was found throughout all the Japanese islands, but positive biases of rMBE in the Hokkaido and Tohoku regions became relatively small. Similar results were found during other seasons in each year.

A map of the relative RMSE (rRMSE) was also constructed and normalized in the same way (i.e., surface-observations) as for rMBE (Figs. 18 and 19). These figures show that rRMSE values around Kyushu and Nansei-islands in western and south-western part of Japan are relatively large. The distribution of rRMSE values during the winter is similar to that during the summer.

Mapping of correlation coefficient between the MSM GHI forecasts and the observations for each season are also shown in Figs. 20–23. The distribution of the correlation coefficient is clearly different from that of

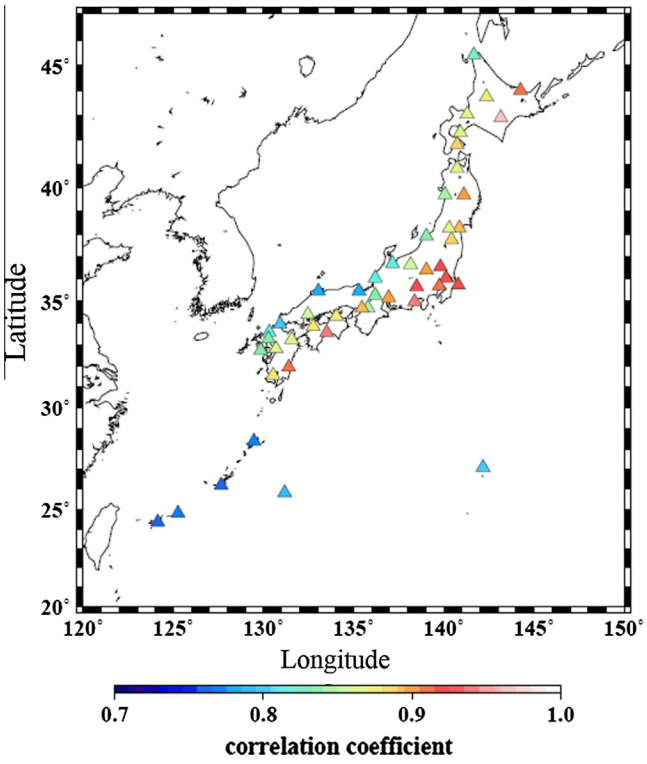

Fig. 20. Map of seasonal GHI correlation coefficient values during winter (DJF) 2012 with an initialization time of 03 h UTC.

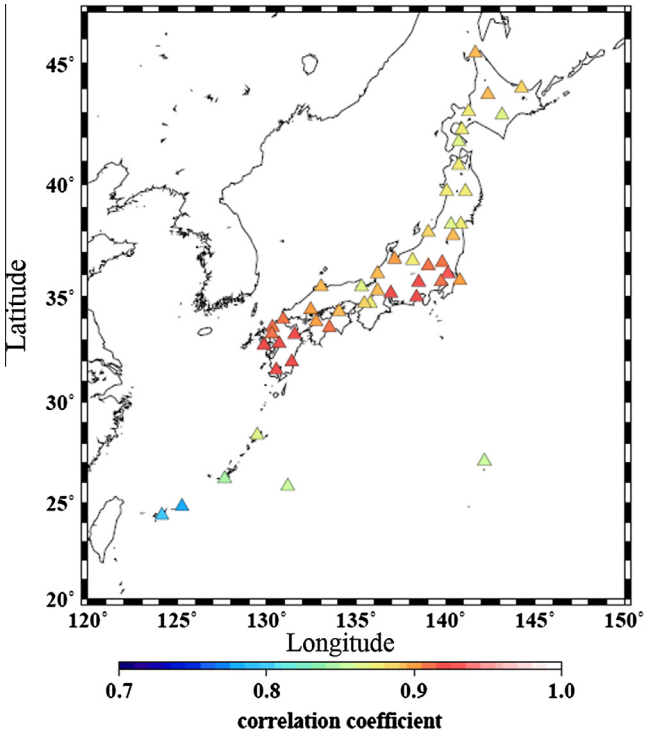

Fig. 21. Same as Fig. 20, but during spring (MAM).

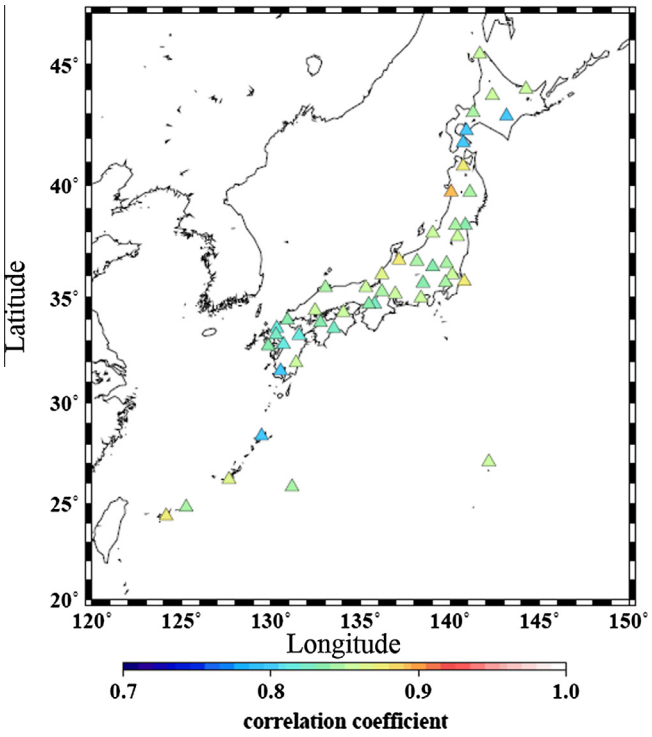

Fig. 22. Same as Fig. 20, but during summer (JJA).

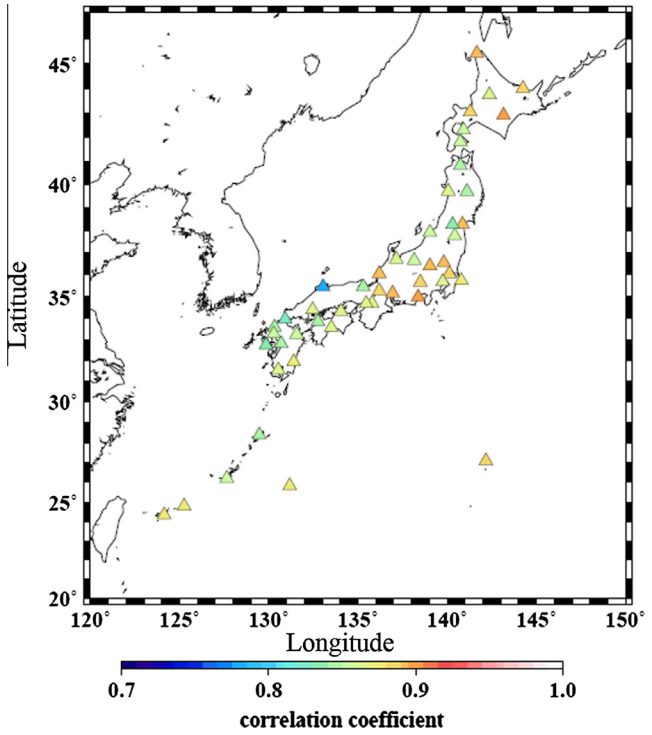

Fig. 23. Same as Fig. 20, but during autumn (SON).

the rMBE and rRMSE. During the winter season (Fig. 20), the correlation coefficient of the JMA observational stations along the Pacific Ocean (Japan Sea) tended to be large (small), because the winter monsoon causes a northwesterly wind flow from the Eurasian continent, which tends to bring clear sky conditions (cloudy and/or overcast) to that region of the Pacific Ocean (Japan Sea). In the southwestern part of Japan (which surrounds

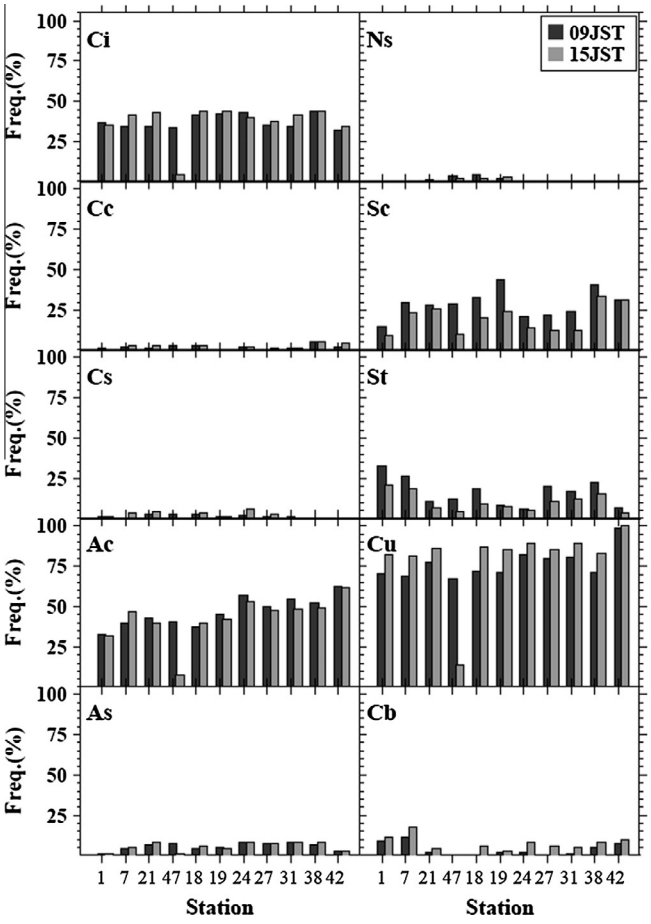

Fig. 24. Frequency of cloud types observed daily at 09 h LST and 15 h LST at JMA stations during 2012. Each box shows the cloud type cirrus (Ci), cirrocumulus (Cc), cirrostratus (Cs), altocumulus (Ac), altostratus (As), nimbostratus (Ns), stratocumulus (Sc), stratus (St), cumulus (Cu), and cumulonimbus (Cb) and JMA station numbers (shown in Fig. 2) are indicated on the horizontal axis.

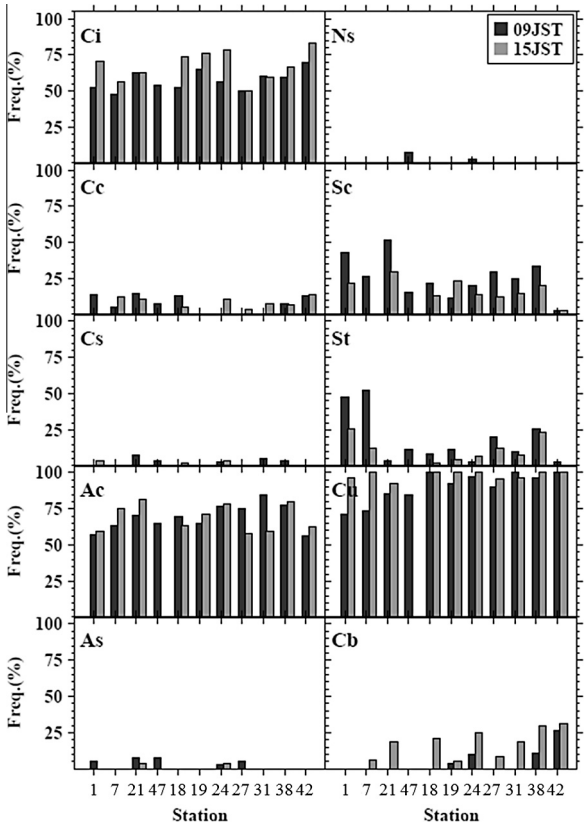

Fig. 25. Same as Fig. 24, but for cases of underestimated GHI during summer (JJA) 2012.

the water), the correlation coefficients were low (about 0.8). During the spring (Fig. 21), relatively large correlation coefficients were found in the Kanto and Kyushu regions. During the summer, the correlation coefficient among all JMA stations tended to be low (about 0.8–0.9, Fig. 22), but during autumn (Fig. 23) the correlation coefficient from the Kanto region to Chubu region became large, once again.

4.3. Influence of cloud type on forecast error

In order to improve the model's microphysical and/or radiation processes, it is necessary to understand which cloud types (i.e., upper-, middle-, and low-level clouds) were monitored during cases in which relatively large GHI forecast errors were found. We screened for cases using the normalized forecast error by surface observations (with a threshold of $0.3 >$ or < -0.3 for each JMA station), and as a result, selected 5–10% of the total cases. The frequency of cloud type occurrences was analyzed for relatively large GHI forecast error cases.

In relation to the underestimations (overestimations) of GHI during summers (winters) over the Kanto region in Japan, Ohtake et al. (2013a) investigated the relationship between GHI forecast errors and the frequency of cloud types (based on observations at the JMA stations over only the Kanto region). They suggested that cirrus, altocumulus, and stratiform type clouds were often observed in relatively large GHI error cases. However, due to the varying climatic conditions in the Japanese islands, the frequency of cloud type occurrences at representative stations during different weather conditions should be analyzed further.

Therefore, we analyzed the occurrence frequency of cloud type using visual monitoring at eleven JMA stations.

First, we analyzed the frequency of cloud types daily for a full year at 09 h LST and 15 h LST during 2012 at the eleven JMA stations (Fig. 24). We selected the eleven stations analyzed in this study (e.g., Sapporo (station number 1, as indicated in Fig. 2 and Table 1), Sendai (7), Niigata (21), Tsukuba (47), Kofu (18), Nagoya (19), Osaka (24), Hiroshima (27), Fukuoka (31), Miyazaki (38), and Ishigakijima (42), shown in Fig. 2 and Table 1) in different climatic regions. Cumulus (Cu) were often observed throughout all selected regions, and in general there was a larger frequency of Cu occurrence in the afternoon (15 h LST) than in the morning (09 h LST). At higher altitudes (~5 km above sea level), cirrus (Ci) were also found

in addition to mid-level altocumulus (Ac) and low-level stratus (Sc). In contrast, the frequency of occurrence of cirrocumulus (Cc), cirrostratus (Cs), altostratus (As), nimbostratus (Ns), and cumulonimbus (Cb) was significantly low (<10%).

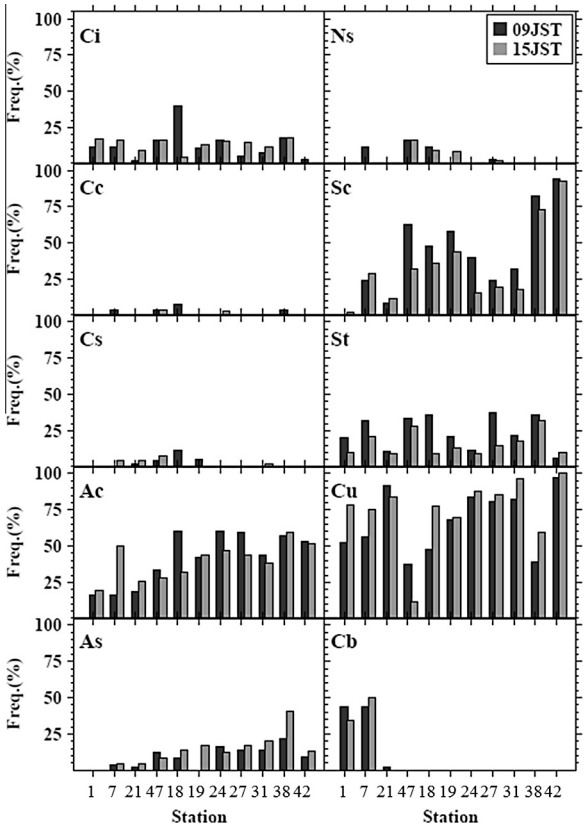

Fig. 26. Same as Fig. 24, but for cases of overestimated GHI during winter (DJF) 2012.

Results showed that in cases in which values were underestimated during the summer of 2012, Cu clouds were found in all negative bias cases (Fig. 25). High-level Ci clouds and mid-level Ac clouds were also observed. However, in cases in which values were overestimated during the winter of 2012, Cu clouds were often observed (Fig. 26); at some JMA stations, Ac and Sc clouds appeared more frequently than other cloud types. In the southwestern part of Japan (i.e., Miyazaki (38) and Ishigakijima (42)), the frequency of Sc (i.e., low-level) cloud observations was relatively high, while the frequency of Ci observations during winter was small compared to summer (Figs. 25 and 26). Regional variations in the occurrence frequency of cloud types in relation to relatively large forecast error cases (i.e., negative biases) were smaller during summer than during winter. A similar tendency regarding the frequency of cloud types in 2012 was also found in other years (2008–2011).

4.4. Case studies for different weather conditions

To better understand the performance of MSM GHI forecasts for various sky conditions, we used several case studies that compare GHI forecasts and observations for clear sky, synoptic scale clouds with a low pressure, and low-level clouds.

Fig. 27a shows a visible satellite image at 12 h JST on October 24, 2012. In this case, clear sky conditions were seen around the Tsukuba station (station number 47 in Fig. 2, yellow square in Fig. 27a). Compared with MSM cloud forecasts, forecasted cloud regions are not found (clear sky conditions) around the Tsukuba station (Fig. 27b). Fig. 27c shows a comparison of the time series of both forecasted and observed GHI values, which

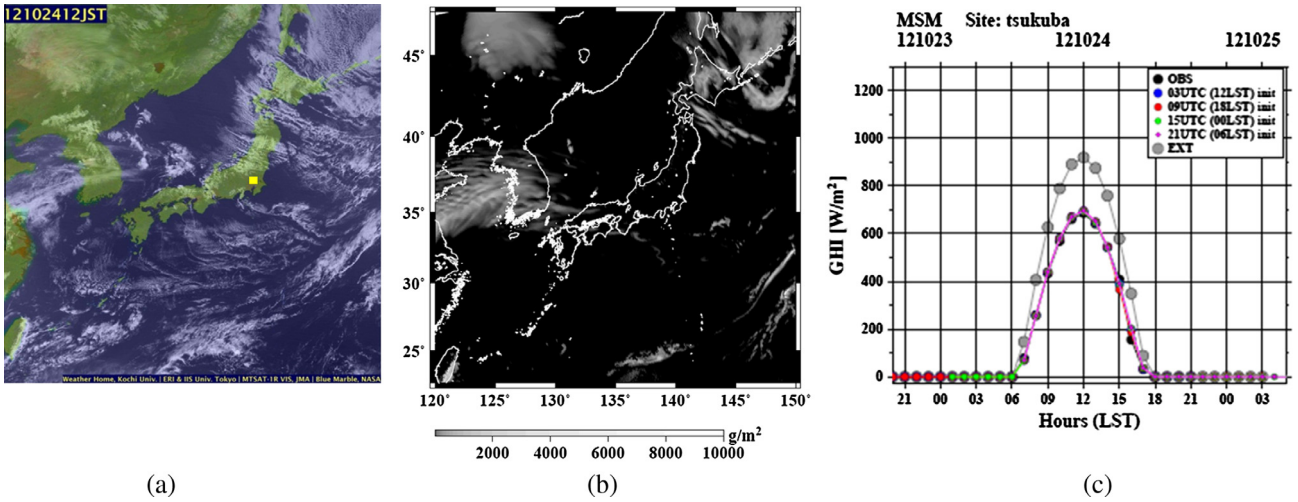

(a) (b) (c)

Fig. 27. (a) MTSAT visible image at 12 h JST on October 24, 2012 and (b) forecasted cloud regions from the initialization time of 03 h UTC (vertical accumulated condensed water substances) from the MSM at the same time. (c) Time series of both observed and forecasted GHI values at the Tsukuba station (shown by the yellow square in (a)) on the same day. Black circles represent hourly GHI observations, and the blue, red, green, and pink lines indicate forecasts from the four initialization times of 03 h, 09 h, 15 h, and 21 h UTC, respectively. Gray circles indicate theoretically calculated extraterrestrial solar irradiance.

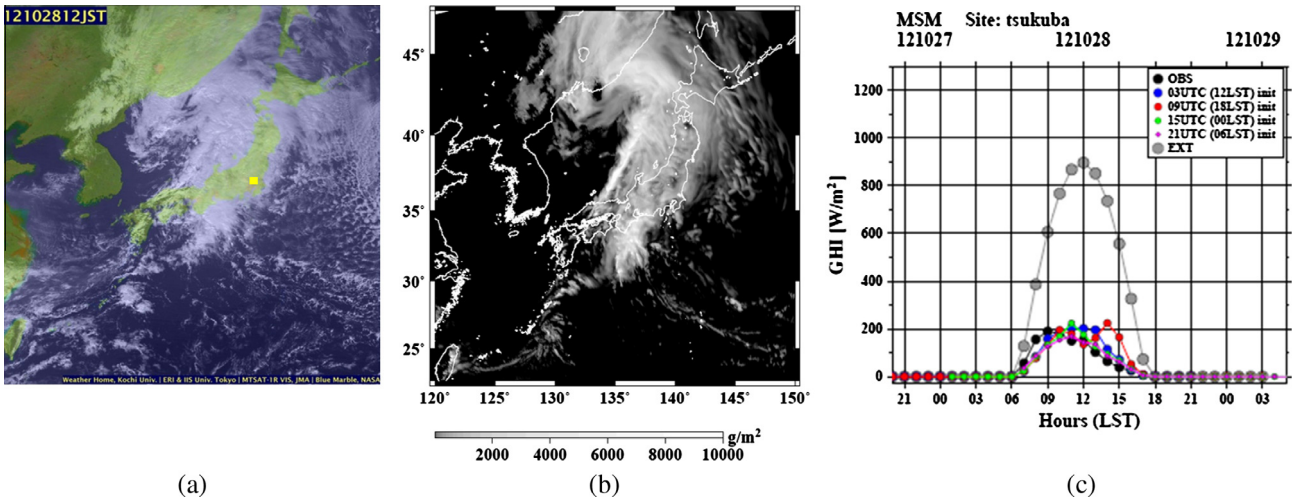

(a) (b) (c)

Fig. 28. Same as Fig. 27, but on October 28, 2012.

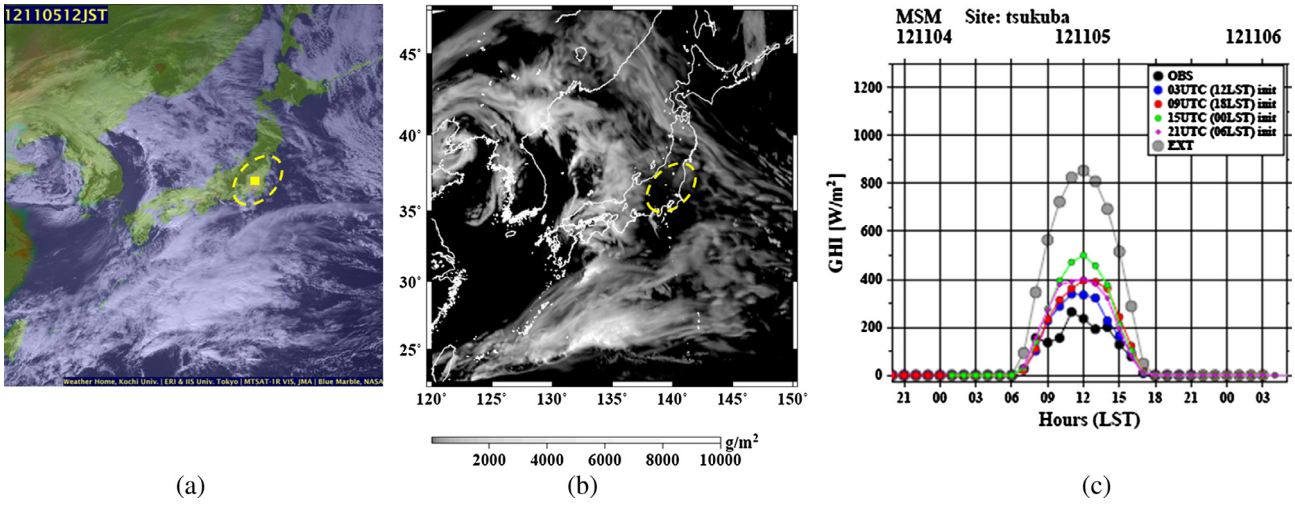

(a) (b) (c)

Fig. 29. Same as Fig. 27, but on November 5, 2012.

indicates that hourly MSM GHI forecasts are significantly close to the observed values.

We also investigated the GHI values on October 28, 2012 (Fig. 28a), a day when synoptic scale clouds (~approximately 1000 km) with a low pressure prevailed throughout all Japanese islands. Compared with satellite-observed clouds around the Japan main islands, MSM cloud regions were similar to the observations (Fig. 28a and b). A time series that shows a comparison of forecasted and observed GHI indicates that the model can forecast hourly GHI values well under the cloud regions (Fig. 28c).

We also conducted a case study using other types of sky conditions, which occurred on November 5, 2012 (Fig. 29a). In this case, the visible satellite image shows low-level clouds in the Kanto region (yellow broken line in Fig. 29a). Sc clouds are also reported by visual monitoring from surface observations at five JMA stations in the same region (not shown). However, MSM cloud regions are disappeared around the Kanto region (Fig. 29b). The GHI forecasts using four different initialization times shows an overestimation in comparison with observations (Fig. 29c).

These results indicate that the MSM cannot reproduce middle- or low-level cumulus clouds (e.g., Ac or Sc) or high-level Ci clouds. Therefore, future improvement in model microphysics and/or radiation processes for each cloud type is necessary.

5. Summary

In the present study, we analyzed the temporal and regional characteristics of GHI forecasts errors from the JMA MSM during the time period from 2008 to 2012. In addition, we also analyzed the frequency of cloud types that occurred over the region that encompasses the Japanese islands in relatively large forecast errors cases.

We found that monthly MBE and RMSE values ranged from −60 to +45 W/m^2 and from 95 to 170 W/m^2, respectively. Maps of MBE values showed that GHI forecast values at all JMA stations were generally underestimated (overestimated) during summer (winter). MBE values were relatively small during both spring and autumn. RMSE values for regional distributions of forecast errors were particularly large in the subtropical climate region (i.e., southern part of the main islands of Japan) along the Pacific Ocean.

The frequency of cloud types over the Japanese islands indicates that regional and seasonal variations in cloud types exist in relatively large GHI forecast error cases. High-level Ci clouds, mid-level Ac clouds and low-level Sc clouds were also observed in cases in which values were underestimated during summer, and overestimated during winter.

Furthermore, from case studies comparing of both forecasted and observed GHI values for several different sky conditions, we confirmed that, in cases of low-level clouds (i.e., stratus), the GHI forecasts from the MSM tended to produce relatively large forecast errors.

Zamora et al. (2003, 2005) compared MM5 (Mesoscale Model 5) radiative fluxes with observations gathered during clear sky conditions, and found that the Dudhia scheme (Dudhia, 1989), which was developed based on the Lacis and Hansen shortwave scheme (Lacis and Hansen, 1974), ignored stratospheric ozone absorption and incorrectly specified aerosol optical depth. The previous study of Lara-Fanego et al. (2012) evaluated GHI forecasts produced by a Weather Research Forecasting model (WRF), i.e., the advanced version of the MM5, using the Dudhia scheme. Their study indicated that, in general, the WRF model overestimated GHI values. Recently, a newest version of the WRF model also has a better solar irradiance parameterization that is similar to radiation schemes used in MSM (e.g., Skamarock et al., 2008).

Previously Nagasawa (2008) showed that systematic negative biases during summer 2006 could be reduced from −200 W/m^2 to −50 W/m^2 during 2007 with the introduction of a partial condensation scheme proposed by Sommeria and Deardorff (1977). However, similar forecast error characteristics (i.e., negative bias) during 2007 were continuously found in our results during the summer from 2008 to 2012. As discussed in Sections 4.3 and 4.4, the accuracy of the GHI forecasts, or the cloud distributions in the MSM, were affected by the reproducibility of each cloud type.

As a future study, it would be desirable to use continuous improvements in the representation of cloud fields for each cloud type in different climatic regions and a modification of associated MSM schemes (i.e., microphysics and radiations schemes) in a modeling study of meteorology fields (e.g., Nagasawa, 2006; Shimose et al., 2013, 2014). Shimose et al. (2014) investigated the forecast accuracy of GHI values obtained by the MSM on the impact of aerosol for cases involving several large forecast errors. They performed sensitivity experiments on the impact of aerosol distribution for GHI forecasts, and suggested that the aerosol optical thickness for cases of aerosol extreme events should not be neglected in the accurate GHI forecast value. However, it is not only the forecast of clouds that requires improvement in the MSM, but also the reproducibility of aerosol distributions. Furthermore, Ohtake et al. (2013b) analyzed the GHI forecast errors and the relationship between forecast errors and weather conditions in order to propose a post-correction of GHI values obtained from the MSM.

For engineering purposes, an understanding of the GHI forecast errors in the present MSM will be helpful in obtaining an accurate forecast of PV power generation. Considerations of both regional and seasonal characteristics of GHI forecast errors will also be useful in planning power supply energy management, including both renewable energy sources and other types of power generation (e.g., thermal power and hydroelectric power).

Acknowledgments

We are grateful to the members of Aerological Observatory and the Numerical Prediction Division of Japan Meteorological Agency (JMA) for their helpful comments concerning the observations and forecast data. We would also like to thank Dr. Christian A. Gueymard of associate editor of Solar Energy and four anonymous reviewers for their helpful comments on the manuscripts. MTSAT visible images were used from the web site of Kochi University (http://weather.is.kochi-u.ac.jp/). This study was carried out in collaboration with the Meteorological Research Institute (MRI) of the JMA and was supported by the New Energy and Industrial Development Organization (NEDO), Japan. Generic Mapping Tools (GMT) and Grid Analysis software were used to draw the figures.

References

Briegleb, B.P., 1992. Delta-Eddington approximation for solar radiation in the NCAR community climate model. J. Geophys. Res. 97, 7603–7612.

Davy, R.J., Troccoli, A., 2011. Interannual variability of solar energy generation in Australia. Sol. Energy 86, 3554–3560. http://dx.doi.org/10.1016/j.solener.2011.12.004.

Dudhia, J., 1989. Numerical study of convection observed during the winter monsoon experiment using a mesoscale two-dimensional model. J. Atmos. Sci. 46, 3077–3107.

Ebert, E.E., Curry, J.A., 1992. A parameterization of ice cloud optical properties for climate models. J. Geophys. Res. 97, D4. http://dx.doi.org/10.1029/91JD02472.

Fonseca Jr., J.G.S., Oozeki, T., Takashima, T., Koshimizu, G., Uchida, T., Ogimoto, K., 2011. Use of support vector regression and numerically predicted cloudiness to forecast power output of a photovoltaic power plant in Kitakyushu. Japan. Prog. Photovolt: Res. Appl. 20, 874–882. http://dx.doi.org/10.1002/pip.1152.

Freidenreich, S.M., Ramaswamy, V., 1999. A new multiple-band solar radiative parameterization for general circulation models. J. Geophys. Res. 104 (D24), 31389–31409.

Ikawa, M., Saito, K., 1991. Description of a non-hydrostatic model developed at the forecast research department of the MRI. Tech. Rep. MRI, 28, 238pp.

Ishikawa, Y., Koizumi, K., 2002. One month cycle experiments of the JMA mesoscale 4-dimensional variational data assimilation (4D-Var) system. CAS/JSC WGNE Res. Activ. Atmos. Oceanic Modell. 32, 0126–0127. http://dx.doi.org/10.2478/mmce-2014-0001.

Kain, J., Fritsch, J., 1993. Convective parameterization for mesoscale models: The Kain–Fritsch scheme. The representation of cumulus convection in numerical models. Meteor. Monogr. 24, 165–170.

Lacis, A.A., Hansen, J.E., 1974. A parameterization for the absorption of solar radiation in the earth's atmosphere. J. Atmos. Sci. 31, 118–133.

Lara-Fanego, V., Ruiz-Arias, J.A., Pozo-Vázquez, D., Santos-Alamillos, F.J., Tovar-Pescador, J., 2012. Evaluation of the WRF model solar irradiance forecasts in Andalusia (southern Spain). Sol. Energy 86, 2200–2217. http://dx.doi.org/10.1016/j.solener.2011.02.014.

Mathiesen, P., Kleissl, J., 2011. Evaluation of numerical weather prediction for intra-day solar forecasting in the continental United States. Sol. Energy 85, 967–977. http://dx.doi.org/10.1016/j.solener.2011.02.013.

Nagasawa, R., 2006. Improvement of a radiation process for the non-hydrostatic model. Proc. of 12th Conference on Atmospheric Radiation, American Meteorological Society, P2-10, <http://ams.confex.com/ams/pdfpapers/113356.pdf>.

Nagasawa, R., 2008. Radiative processes. Report of Numerical Prediction Division 54, 149–165 (in Japanese, Suuchiyohouka Bessatsu Houkoku).

Ohmori, S., Yamada, Y., 2004. Implementation of the Kain-Fritsch convective parameterization scheme in the JMA's Non-hydrostatic Model. CAS/JSC WGNE Res. Activ. Atmos. Oceanic Modell. 34, 0425–0426.

Ohtake, H., Shimose, K.-I., Fonseca Jr., J.G.S., Takashima, T., Oozeki, T., Yamada, Y., 2013a. Accuracy of the solar irradiance forecasts of the Japan Meteorological Agency mesoscale model for the Kanto region, Japan. Sol. Energy 98. Part B, 138–152. http://dx.doi.org/10.1016/j.solener.2012.10.007.

Ohtake, H., Shimose, K.-I., Fonseca Jr., J.G.S., Takashima, T., Oozeki, T., Yamada, Y., 2013b. Range of forecast errors of global irradiance by the Japan Meteorological Agency numerical weather prediction model for the PV power forecast, Proceedings of 28th European Photovoltaic Solar Energy Conference and Exhibition (EU PVSEC), Paris, France, pp. 3638–3643, http://dx.doi.org/10.4229/28thEUPVSEC2013-5AO.9.3.

Ou, S.C., Liou, K.N., 1995. Ice microphysics and climate temperature feedback. Atmos. Res. 35, 127–138.

Pelland, S., Galanis, G., Kallos, G., 2011. Solar and photovoltaic forecasting through post-processing of the global environmental multiscale numerical weather prediction model. Prog. Photovolt. Res. Appl. 22, 284–296. http://dx.doi.org/10.1002/pip.1180.

Perez, R., Kivalov, S., Schlemmer, J., Hemker, K., Renné, D., Hoff, T., 2010. Validation of short and medium term operational solar radiation forecasts in the US. Sol. Energy 84, 2161–2172. http://dx.doi.org/10.1016/j.solener.2010.08.014.

Saito, K., Fujita, T., Yamada, Y., Ishida, J., Kumagai, Y., et al., 2006. The operational JMA nonhydrostatic mesoscale model. Mon. Weather Rev. 134, 1266–1298. http://dx.doi.org/10.1175/MWR3120.1.

Saito, K., Ishida, J., Aranami, K., Hara, T., Segawa, T., et al., 2007. Nonhydrostatic atmospheric models and operational development at JMA. J. Meteor. Soc. Japan 85B, 271–304.

Shimose, K.-I., Ohtake, H., Fonseca Jr., J.G.S., Takashima, T., Oozeki, T., Yamada, Y., 2013. Improvement of the cloud scheme of the Japan Meteorological Agency mesoscale model for the forecasting the photovoltaic power production. In: Proc. of the 28th EU PVSEC, http://dx.doi.org/10.4229/28thEUPVSEC2013-5BV.4.28.

Shimose, K.-I., Ohtake, H., Fonseca Jr., J.G.S., Takashima, T., Oozeki, T., Yamada, Y., 2014. Impact of aerosols on the forecast accuracy of solar irradiance calculated by a numerical weather model. Eur. Phys. J. Special Topics 223, 2621–2630. http://dx.doi.org/10.1140/epjst/e2014-02213-0.

Skamarock, W.C., Klemp, J.B., Dudhia, J., Gill, D.O., Barker, D.M., Duda, M.G., Huang, X-Y., Wang, W., Powers, J.G., 2008. A description of the Advanced Research WRF version 3, NCAR TECHNICAL NOTE. NCAR/TN-475+STR, Mesoscale and Microscale Meteorology Division, National Centre for Atmospheric Research, Boulder, USA.

Slingo, A., 1989. A GCM parameterization for the shortwave radiation properties of water clouds. J. Atmos. Sci. 46, 1419–1427.

Sommeria, G., Deardorff, J.W., 1977. Subgrid-scale condensation in models of nonprecipitating clouds. J. Atmos. Sci. 34, 344–355.

Yoshida, R., Sawada, M., Yamazaki, T., Iwasaki, T., 2011. Verification of nonhydrostatic-model simulated radiation Using in situ observational data in Miyagi, Yamagata and north part of Fukushima prefectures. Tenki 58, 599–605 (in Japanese).

Zamora, R.J., Solomon, S., Dutton, E.G., Bao, J.W., Trainer, M., Portmann, R.W., White, A.B., Nelson, D.W., McNider, R.T., 2003. Comparing MM5 radiative fluxes with observations gathered during the 1995 and 1999 Nashville southern oxidant studies. J. Geophys. Res. 108 (D2), 4050.

Zamora, R.J., Dutton, E.G., Trainer, M., McKeen, S.A., Wilczak, J.M., Hou, Y.T., 2005. The accuracy of solar irradiance calculations used in mesoscale numerical weather prediction. Mon. Weather Rev. 133, 783–792. http://dx.doi.org/10.1175/MWR2886.1.